2014 Canada-China Conference on Advanced Reactor Development (CCCARD-2014)
Niagara Falls Marriott Fallsview Hotel & Spa, Niagara Falls, Ontario Canada, April 27-30, 2014.

CCCARD2014-017

Microstructural Characterization of Oxide Scales Grown on Austenitic Fe-Cr-Ni Alloys Exposed to Supercritical Water (SCW)

S. Mahboubi, G. Botton and J. Kish
Department of Materials Science and Engineering, McMaster University, 1280 Main Street West, Hamilton, ON, CA
mahbos@mcmaster.ca, gbotton@mcmaster.ca, kishjr@mcmaster.ca

Abstract

The goal of this study is to compare the corrosion resistance of Alloy 800 HT and Alloy 3033 in supercritical water (SCW). Test coupons were exposed to 25 MPa SCW at 550 °C for 500 h in a static autoclave. Gravimetric measurements showed a significantly higher corrosion resistance of Alloy 3033 compared with Alloy 800 HT and Type 316L stainless steel. Electron microscopic examination revealed the improved corrosion resistance related to the structure and composition of the oxide scales formed. Optimum corrosion resistance was imparted by a single thin chromia (Cr_2O_3) layer, as observed on Alloy 3033.

1 Introduction

Supercritical water (SCW) is a state in which the temperature and the pressure of water is above 374.15 °C and 22.1 MPa respectively [1]. Such an environment is inherent to one of the six Generation IV reactor designs being considered: namely the supercritical water-cooled reactor (SCWR) [2]. As a coolant, SCW heated to a high outlet temperature (500-625 °C) is expected to increase the thermodynamic efficiency of SCWR as high as 50% if steam reheat is used [2-4]. As a result, the selection of construction materials such as the cladding for the fuel that can perform at such high temperatures while being resistant to corrosion damage has been an important challenge [2]. Most of the previous studies on candidate fuel cladding materials for SCWR design have focused on the formation of corrosion resistance of conventional austenitic stainless steels, such as Type 304L and 316L. In these studies it has been consistently revealed that oxide scales formed consist of a double layer; namely an inner protective Fe-Cr spinel ($FeCr_2O_4$) and an outer non-protective magnetite (Fe_3O_4) scale [5-11].

It is well known that the high temperature (below 1000 °C) oxidation (corrosion) resistance of austenitic stainless steel relies on the Cr content; with an increase in Cr content leading to improved corrosion resistance [12]. The optimum corrosion resistance depends on the formation of a protective chromia (Cr_2O_3) layer and whether this Cr_2O_3 layer is adherent and free of short-circuit diffusion paths (e.g. pores) that increase diffusion of ions through the scale [12,13]. The diffusion of ions through such a protective scale has received some attention, but further studies are necessary [12]. It has been experimentally reported that an alloyed Cr content of higher than

25 wt% is needed to prevent the formation of an outer $FeCr_2O_4$ layer on top of an inner Cr_2O_3 layer, resulting in optimum corrosion resistance [14].

In the current research, the corrosion resistance of austenitic stainless steel, Incoloy Alloy 800 HT (~20 wt% Cr) and Nicrofer Alloy 3033 (~33 wt% Cr) in SCW are subjected to study. The aim is to relate the observed corrosion resistance to the structure and composition of the oxide scale formed on each alloy. Reported studies on the corrosion resistance of Alloy 800 HT in SCW show that the increased alloyed Cr content relative to Type 304L/316L stainless steel does lead to improved corrosion resistance [15,16]. Electron microscopy techniques were used to examine the structure and composition of the oxide scales formed on each alloy. Electron energy-loss spectroscopy (EELS) was chosen as the major method of analysis. This technique can distinguish the difference between oxides types by comparing the position and relative height of elemental peaks, which depends on the electronic structure and valence state [3]. The relative difference in corrosion resistance observed was rationalized using oxide scale growth concepts developed for austenitic stainless steels from high temperature oxidation studies. This comparison is considered meaningful since the corrosion behavior exhibited by austenitic stainless steel in SCW has been shown to be similar to that exhibited in low pressure superheated steam [2,17].

2 Experimental Procedure

2.1 Material

Rectangular test coupons of Alloy 800 HT (20×10×1 mm) and Alloy 3033 (25×5×1 mm) were prepared from commercial cold-rolled and annealed plate using a diamond wheel saw. The composition of the alloys is listed in Table 1. The Alloy 800HT plate had an ASTM E112 grain size of 4, whereas the Alloy 3033 plate had an ASTM E112 grain size of 5. In order to ease mounting on the coupon tree, a 2 mm diameter hole was drilled out near the top of each coupon. Coupons were manually ground to an 800 grit surface finish using SiC abrasive papers and water as a lubricant, rinsed with ethanol and then dried with a hot air stream. The dimensions and weight of each coupon was measured using digital calipers and analytical balance, respectively, prior to immersion.

Table 1 Composition (wt%) of Alloy 800 HT and Alloy 3033

Alloy	Fe	Cr	Ni	C	Mn	Si	Cu	Ti	Al	Mo	N	Ce	S	P	Co
800 HT	Bal.	20.6	30.7	0.07	0.6	0.3	0.03	0.6	0.5	-	-	-	<0.01	0.01	0.03
3033	Bal.	33.4	31.9	0.01	0.6	0.2	0.5	<0.01	-	1.5	0.4	0.02	-	-	-

2.2 SCW Corrosion Testing

A static autoclave testing facility (CanmetMATERIALS) with the total chamber volume of 1045 ml was used. A set of four manually ground coupons were suspended on a coupon tree and exposed to ASTM 1193 Type IV deionized water with the density of 85.168 kg/m^3, the pressure

of 25 MPa and the temperature of 550 °C for 500 h. The initial dissolved oxygen content in the water was 8 ppm. No attempt was made to maintain this level during the 500 h exposure.

2.3 Weight Change Measurement

Each coupon was weighed before and after exposure using an analytical balance with the precision of 0.001 mg in order to determine the amount of weight gained (or lost) during the 500 h exposure. A weight loss measurement was conducted using one coupon from each set of four in order to confirm the comparative results of the weight gain. Only one coupon was selected in order to save the remaining for the electron microscopy examination of the oxide scale formed. The oxide scale was removed by first immersing the coupon in a citric acid, dibasic ammonium citrate and disodium EDTA solution and then immersing in a potassium permanganate and caustic soda solution. The effectiveness of this procedure has been demonstrated elsewhere [2].

2.4 Electron Microscopy Examination

Scanning electron microscopy (SEM) was initially used for a plan view analysis of the nature and morphology of the oxide scale formed on both alloys. This was done using a JEOL JSM-7000F microscope equipped with a Schottky Field Emission Gun (FEG) filament and an integrated Oxford Synergy system with INCA EDS X-ray micro-analysis using an accelerating voltage of 10 kV and a working distance of 10 mm.

Site-specific thin cross-section foils were prepared from a corroded Alloy 800 HT and Alloy 3033 coupon surface using Zeiss NVision 40 focused ion beam (FIB) with a gallium (Ga) ion beam voltage of 30 k, a current beam of 80 pA and a working distance of 5.6-5.9 mm. A tungsten (W) strap (2 μm thick) was deposited on the coupons to protect the oxide scale during ion milling. Subsequent examination using transmission electron microscopy (TEM) was conducted using JEOL 2010F TEM/STEM operating at 200 kV. Energy dispersive spectroscopy (EDS) was applied on FIB-prepared cross-section foil in scanning transmission electron microscopy (STEM) mode in order to achieve elemental composition.

EELS, with a dispersion of 0.2 eV/pixel, was done for microstructural characterization of the oxide scales. While the O, Cr, Fe and Ni edges can all be used for oxide analysis, the O edge typically shows more variation in each oxide type which makes the analysis more straight forward. However, in the case of α-Fe_2O_3, γ-Fe_2O_3 and Fe_3O_4 where the EELS spectra look quite similar with each other, the position and intensity of the peak identified with the symbol (●) relating to the coordination of O atoms in each compound can be helpful [3]. Figure 1 shows the difference between the O edges for distinct Fe oxides (a-d) and O and Cr edges for the Cr-rich oxides (e,f) [3,18]. These spectra are used in the current work as reference for further investigation.

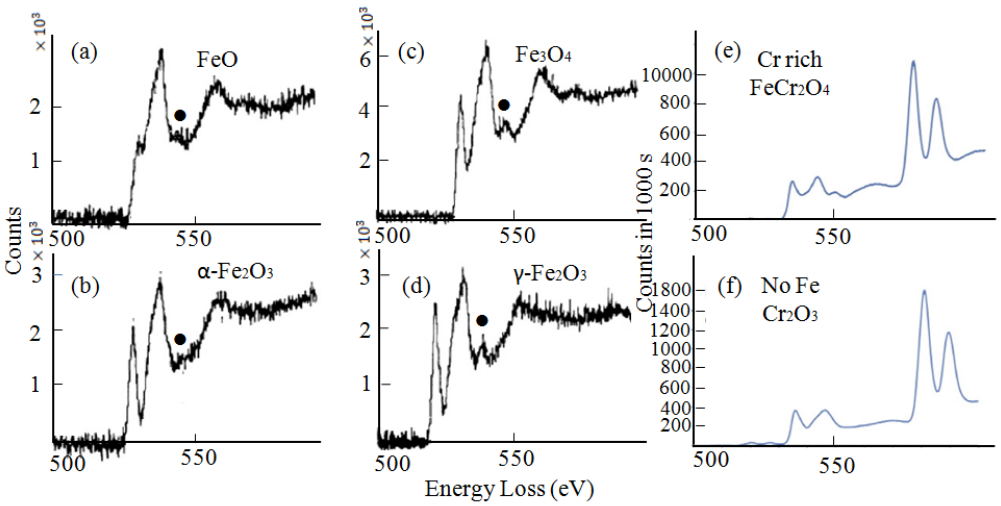

Figure 1 EELS O edge spectra for a. FeO, b. α-Fe_2O_3, c. Fe_3O_4, d. γ-Fe_2O_3, and O K and Cr L edge spectra in reference compounds and for (e) $FeCr_2O_4$ and (f) Cr_2O_3 [3,18].

Auger electron spectroscopy (AES) was performed with JEOL JAMP-9500 F AUGER/FE-SEM on three different surface areas of each alloy to confirm the previous results obtained by TEM. Before the AES analysis, coupons were cleaned to remove the residual contamination by sputtering argon (Ar) ion beam of 3 kv for 30 s. Coupons were then analyzed using a 3 kV Ar ion beam with a 30 degrees tilting angle and a working distance of 20-23 mm. Moreover, standard deconvoluted curves were used for each expected compounds in order to fit the peaks and characterize them.

3 Results

Figure 2 shows the weight change measurement for Alloy 800 HT and Alloy 3033 exposed in SCW at 550 °C for 500 h compared with Type 316L stainless steel after exposure in the same condition [7]. Positive weight change (weight gain) data was obtained by calculating the average for each set of four coupons, whereas the negative weight change (weight loss) data was obtained for only one coupon from each set of four coupons. Alloy 3033 with the highest alloyed Cr content (33.4 wt%) showed the least weight gain (WG) and weight loss (WL) followed by Alloy 800 HT with intermediate alloyed Cr (20.6 wt%) and then by Type 316L stainless steel with the lowest alloyed Cr content (16.3 wt%) [7].

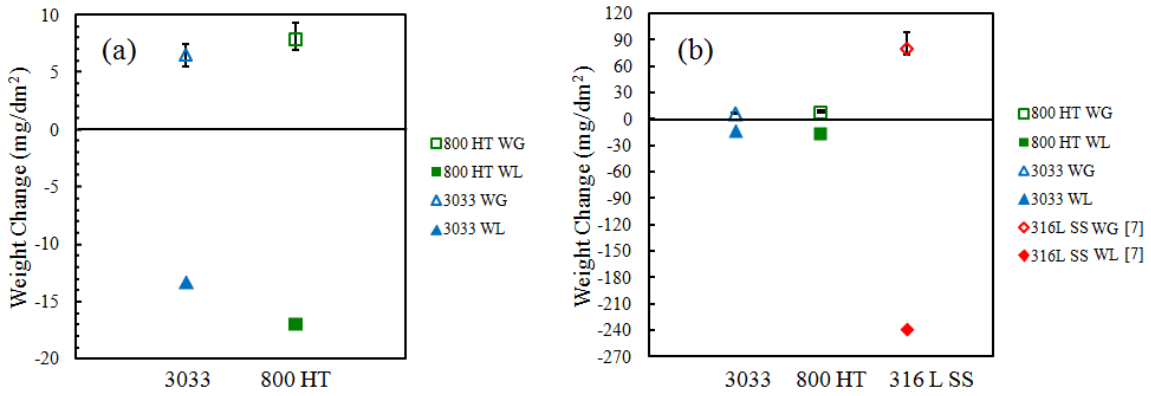

Figure 2 Weight change comparison of (a) Alloy 800 HT and Alloy 3033 and (b) Alloy 800 HT, Alloy 3033 and Type 316L stainless steel [7] exposed in SCW at 550 °C for 500 h.

Figure 3 shows a typical SEM plan view image of an Alloy 800HT and Alloy 3033 coupon surface after exposure to SCW at 550 °C for 500 h. The oxidized surface on Alloy 800 HT [Figure 3(a)] consisted of particles with spinel structure embedded on a uniform oxide scale. An SEM/EDS analysis on the particles showed they are enriched in O and Fe. The SEM/EDS analysis on the uniform oxide scale was considered not to be trustworthy since the interaction volume of the electrons interacting with the coupon was expected to be much larger than the thickness of the oxide scale. Figure 3(b) shows the oxide scale formed on Alloy 3033 was much more uniform and compact. Also scattered particles enriched in silver (Ag) and others enriched in cerium (Ce) were observed. The Ag particles were most likely an artifact from the autoclave testing since an Ag plated gasket was used to seal the autoclave lid. As shown in Figure 6, the Ce particles were likely oxide inclusions resulting from the steelmaking process. Therefore, neither particle is expected to have had any influence whatsoever of the formation of the protective oxide scale.

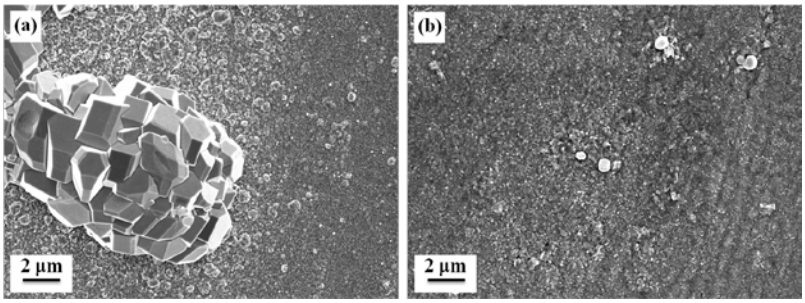

Figure 3 Plan view SEM images of (a) Alloy 800 HT coupon and (b) Alloy 3033 coupon exposed in SCW at 550 °C for 500 h.

In order to analyze both particles and the uniform oxide scale areas on which the particles are embedded, the site-specific TEM sample preparation via FIB milling was chosen in the manner depicted in Figure 4.

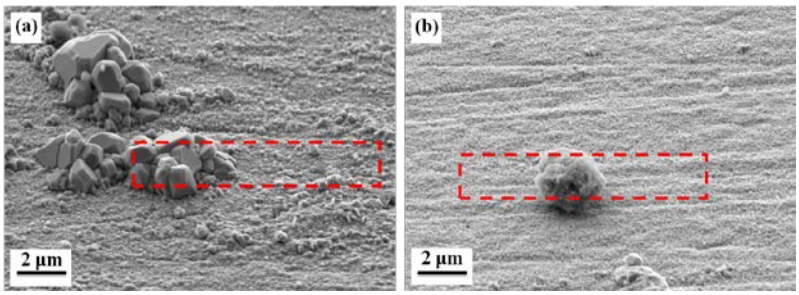

Figure 4 Plan view FIB/SEM images showing an area of interest, framed with a dashed rectangle, for TEM sample preparation of an (a) Alloy 800 HT coupon and (b) Alloy 3033 coupon exposed in SCW at 550 °C for 500 h.

Figure 5 shows a bright field STEM image of the thin cross-section foil along with the EDS elemental map for Alloy 800 HT. The particles on the oxide scales were enriched in Fe and O which is consistent with the results from SEM/EDS analysis. Also an internal oxidation enriched in Fe, Cr and O was formed in the alloy. The "clean" areas of oxide (with no particles on top) consisted of a top layer enriched in Fe and O and the layer beneath enriched in Cr and O. Ni was enriched at the alloy/oxide interface. This may be due to either the lower diffusion coefficient of Ni in the oxide scale in comparison with Fe and Cr or the low O_2 potential of the SCW environment where potential is less than Ni/NiO equilibrium [6]. Areas of Cr depletion were observed near the alloy/oxide interface. This was likely due to the outward diffusion of Cr.

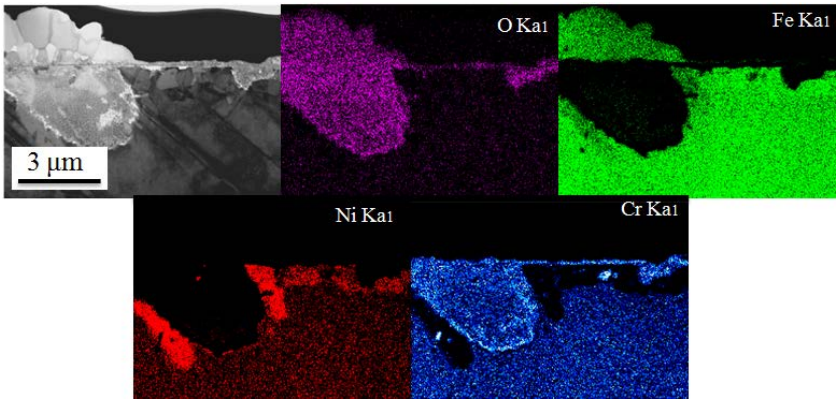

Figure 5 Bright-field STEM image and STEM/EDS elemental maps for O, Fe, Ni and Cr of the corroded Alloy 800 HT surface after exposure in SCW at 550 °C for 500 h.

Figure 6 shows a bright-field STEM image of the thin film sample along with the EDS elemental map for Alloy 3033. The particle on the oxide scale was confirmed to be Ce-enriched. Also the areas underneath the particle were rich in both Ce and O. It is concluded that this particle was an oxide inclusion resulting from the steelmaking practice. Cerium is not an intentional alloying element of Alloy 3033. In contrast with the results of Alloy 800 HT, the "clean" areas of oxide scale formed on Alloy 3033 included only one layer which was enriched in Cr.

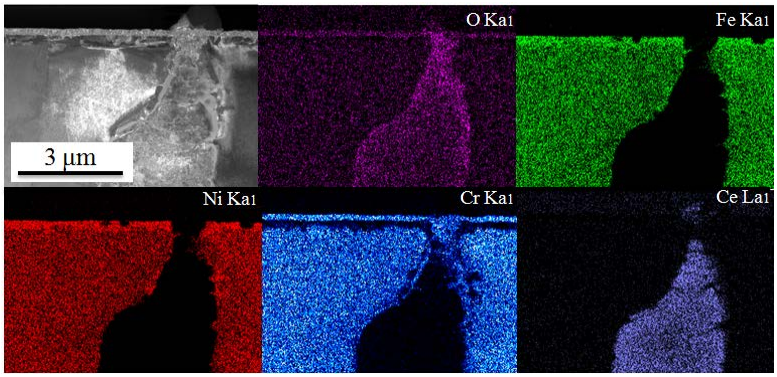

Figure 6 Bright-field STEM image and STEM/EDS elemental maps for O, Fe, Ni, Cr and Ce of corroded Alloy 3033 surface after exposure in SCW at 550 °C for 500 h.

Figure 7 shows the bright-field STEM image and the analysis of three selected areas of the particle embedded on the uniform oxide scale formed on the Alloy 800 HT coupon. EELS was conducted on this particle and the internal oxide area underneath it. The results indicated that the particle consisted of an outer Fe_3O_4 layer (external oxidation) residing on an inner $FeCr_2O_4$ spinel (internal oxidation) .

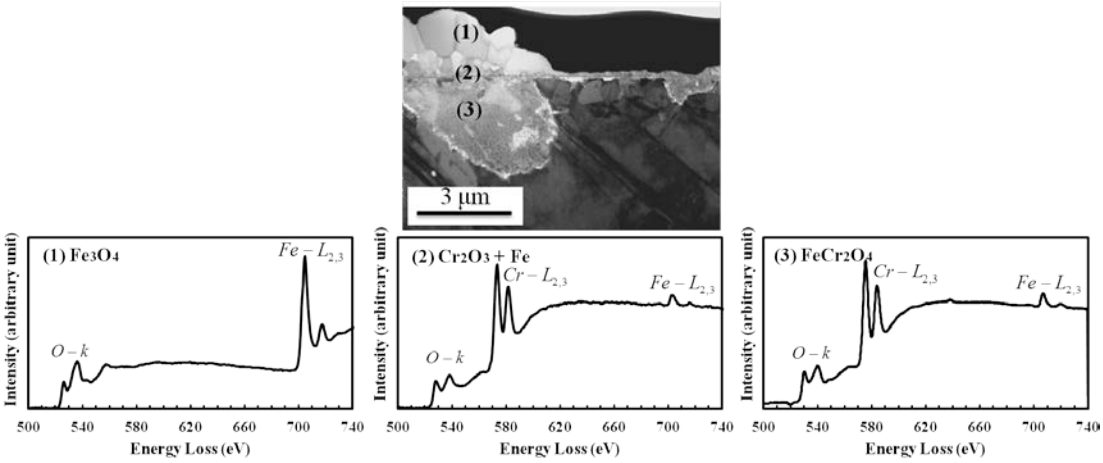

Figure 7 Bright-field STEM image and the corresponding EELS analysis of the particle embedded on the uniform oxide scale formed on the Alloy 800 HT coupon.

Figure 8 shows a high magnification dark-field STEM image and the corresponding EELS analysis of the adjacent “clean” area of oxide formed on Alloy 800 HT. The results reveal that the oxide scale was comprised of an outer $FeCr_2O_4$ spinel layer residing on top of a Cr_2O_3 inner layer. Moreover, several pores were observed in the scale especially at the alloy/oxide interface and the $Cr_2O_3/FeCr_2O_4$ interface.

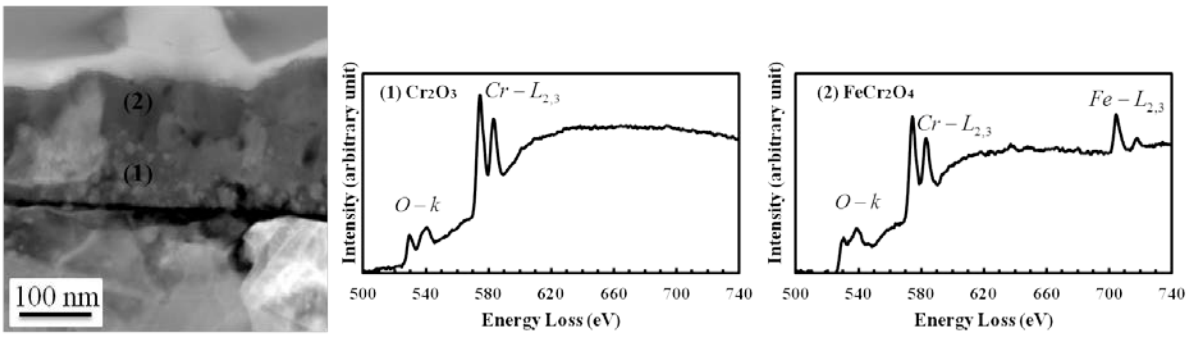

Figure 8 High magnification dark-field STEM image and the corresponding EELS analysis of the oxide scale formed on Alloy 800 HT exposed to SCW at 550 °C for 500 h.

As shown in Figure 9, the EELS data reveal that just a single layer of Cr_2O_3 formed on Alloy 3033. No Fe edge was observed in the spectrum. In addition, the Cr_2O_3 layer was more compact and contained less pores than Cr_2O_3 layer formed on Alloy 800 HT.

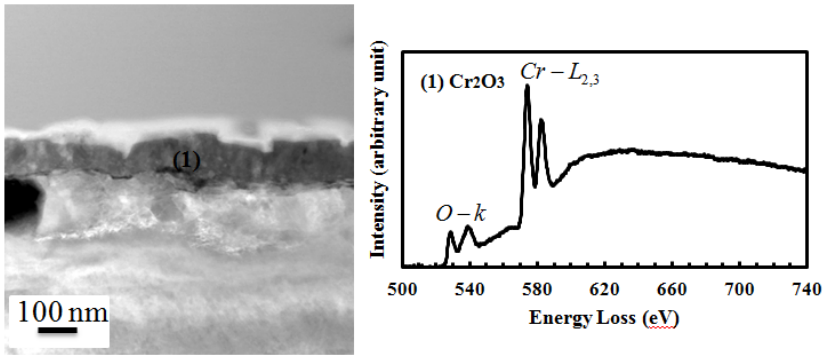

Figure 9 High magnification dark field STEM image and the corresponding EELS analysis of the oxide scale formed on Alloy 3033 exposed to SCW at 550 °C for 500 h.

Since the TEM analysis was only obtained from a very small region of the surface of just one coupon, it was necessary to confirm the above observations using AES. Figure 10 shows the depth profile through the “clean” oxide formed on each alloy after exposure to SCW at 550 °C for 500 h. The depth profiles agreed well with the EELS data, confirming a double layer of oxide formed on Alloy 800 HT and a single layer of oxide formed on Alloy 3033.

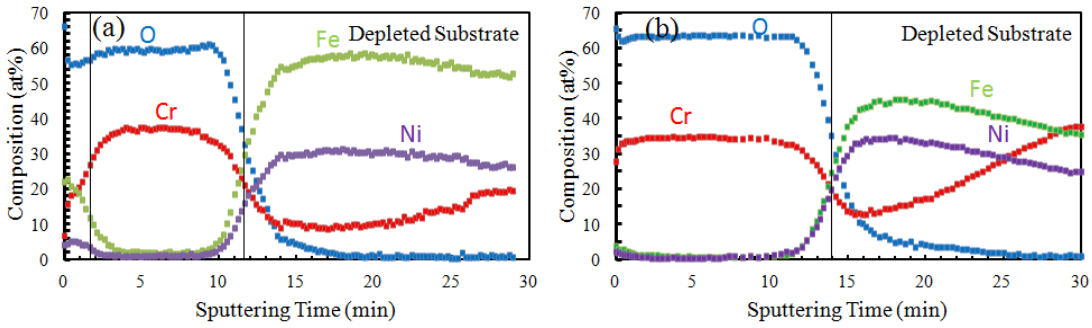

Figure 10 AES depth profile of (a) Alloy 800 HT and (b) Alloy 3033 exposed to SCW at 550 °C for 500 h.

4 Discussion

Figure 11 shows a schematic summary of the oxide scales formed on three different candidate austenitic Fe-Cr-Ni alloys after exposure to SCW. The higher alloyed Cr content in Alloy 800 HT and Alloy 3033 promotes the formation of a Cr_2O_3 layer. Given the marked reduction in the weight change measurements these two alloys exhibited in comparison with Type 316L stainless steel, the Cr_2O_3 layer is concluded to play a controlling role in imparting corrosion resistance. The improved corrosion resistance coincides with a marked reduction in the oxide scale thickness, which decreased from a typical value of 20-40 μm (20,000-40,000 nm) on Type 304L/316L stainless steels [5-11] down to about 200 nm on Alloy 800 HT and 100 nm on Alloy 3033. The key questions are: (i) why does a Cr_2O_3 scale form on Alloy 800 HT and on Alloy 3033 and not on Type 316L stainless steel, and (ii) why does a spinel $FeCr_2O_4$ outer layer form on Alloy 800 HT and not on Alloy 3303? To answer these questions, it was instructive to consider oxide scale growth concepts developed for austenitic stainless steels from high temperature oxidation studies. This comparison is considered meaningful since the corrosion behavior exhibited by austenitic stainless steel in SCW has been shown to be similar to that exhibited in low pressure superheated steam [2,17].

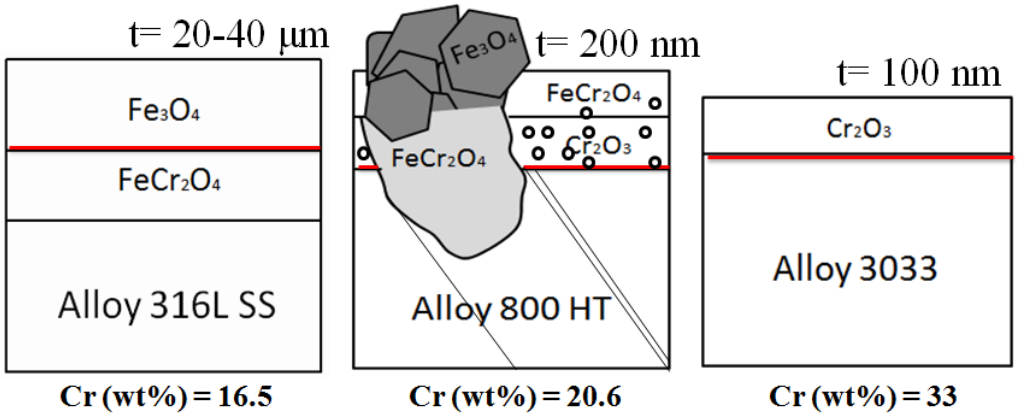

Figure 11 Summary of microstructural characterization of the oxide scales formed on Type 316L stainless steel [7], Alloy 800 HT and Alloy 3033 exposed to SCW at 550 °C for 500 h.

In Fe-Cr-O and Ni-Cr-O systems, the presence of Cr_2O_3 precipitates near the alloy/scale interface has been observed depending on the temperature of exposure [14]. In Fe-20Cr system however, as the oxide scale grows laterally, the Cr_2O_3 precipitates incorporate into the scale and transforms into $FeCr_2O_4$ [14]. Diffusion of elements into spinel $FeCr_2O_4$ layer, albeit relatively slow, is meaningful. The higher diffusion co-efficient of Fe promotes the formation of an outer Fe_3O_4 layer on top of the spinel $FeCr_2O_4$ layer.

An increase in the alloyed Cr content (from ~16.5 wt% Cr to 20.6 wt% Cr) causes a formation of more continuous Cr_2O_3 layer on the surface due to outward diffusion of Cr where O diffusion also incorporates in oxide formation [14]. Kofstad [19] showed that the inward diffusion of O into the scale is approximately three orders of magnitude slower than outward diffusion of Cr into the scale [20]. This leads to the formation of an external Cr_2O_3 scale. Moreover, during the growth of a Cr_2O_3 scale on Fe-based alloys, Fe diffuses through the scale readily since the Fe^{3+} radius (0.065 nm) is very close to Cr^{3+} radius (0.062 nm) [12,21]. Measurements of the diffusion profiles of Fe in the polycrystalline Cr_2O_3 at 900 °C as reported by Sabioni et al. reveal two different regions: (i) an effective diffusion region (incorporates with the inner oxide layer in Alloy 800 HT and Alloy 3033 in this research) that encompasses both bulk and grain boundary diffusion (for Cr_2O_3 grain size < 1 μm) and (ii) an outer oxide layer encompassing just grain boundary diffusion region [12]. Therefore, both diffusion domains need to be considered in the growth process of Cr_2O_3 [12]. Furthermore, studies by Lobnig et al. [14,22] on the effective values of Fe and Cr diffusion coefficient in the Cr_2O_3 scale at 900 °C for Fe-20Cr alloys shows D_{eff} (Fe) ≈ D_{eff} (Cr), which can explain the fast growth of $FeCr_2O_4$ on Cr_2O_3 layer (as observed on Alloy 800 HT in this study). The presence of pores in the oxide scale on Alloy 800 HT (as revealed in Figure 8) can accelerate Fe diffusion in the oxide scale. The AES results in Figure 10

also suggest that a very small concentration of Ni also diffused out through the oxide scale, likely for the same reason argued for Fe. What prevents the formation of $FeCr_2O_4$ on the Cr_2O_3 layer formed on Alloy 3033 is likely related to the increased alloyed Ni/Fe. Such an increased ratio has been reported to reduce the Fe activity and, correspondingly the solubility of Fe in Cr_2O_3 [14]. It has been experimentally reported that a Cr concentration of higher than 25 wt% is needed to prevent the formation of $FeCr_2O_4$ [14].

Based on the gravimetric measurements and the electron microscopy analyses, an alloy Cr content in excess of 25 wt.% ensuring the formation of a single Cr_2O_3 layer is necessary for optimum corrosion resistance in SCW. The formation of the internal oxidation grown in Alloy 800 HT is likely a result of the enhanced short-circuit diffusion along grain boundary and dislocation network clusters. It has been reported that a higher population of dislocation clusters relative to grain boundary area can enhance the likelihood of internal oxidation in Alloy 800 HT [23]. An inner layer $FeCr_2O_4$ layer is undesirable as it has a strong tendency to permit significant Fe diffusion (and subsequent corrosion).

5 Conclusion

- Gravimetric measurements and electron microscopy techniques were successfully used to relate the corrosion resistance of austenitic Fe-Cr-Ni alloys in SCW (25 MPa SCW at 550ºC) to the structure and composition of the oxide scale formed.
- The corrosion resistance increased in the expected manner with an increase in the alloyed Cr content (Alloy 3033> Alloy 800 HT> Type 316L). The more protective oxide scale was comprised of a single layer of Cr_2O_3 (Alloy 3033) and the least protective was comprised on a Fe_3O_4 layer residing on top of an inner $FeCr_2O_4$ spinel layer (Type 316L stainless steel).
- An alloyed Cr content in excess of 20 wt.% is required to promote the formation of a single layer of Cr_2O_3. Although the alloyed Cr content of about 20 wt.% in Alloy 800 HT was sufficient to promote the formation of an Cr_2O_3 scale, it was insufficient to hinder the formation of a spinel $FeCr_2O_4$ outer layer.

6 Acknowledgements

The authors would like to acknowledge the funding to Canada Gen-IV National Program was provided by Natural Resources Canada through the Office of Energy Research and Development, Atomic Energy of Canada Limited, and Natural Sciences and Engineering Research Council of Canada. Also special thanks to CanmetMATERIALS for conducting the SCW corrosion testing.

7 References

[1] M. Sun, X. Wu, Zh, Zhang and E.H. Han, "Oxidation of 316 stainless steel in supercritical water", *Corrosion Science*, Vol. 51, 2009, pp. 1069-1072.
[2] D.A. Guzonas and W.G. Cook, "Cycle chemistry and its effect on materials in a supercritical water-cooled reactor: A synthesis of current understanding", *Corrosion Science*, Vol. 65, 2012, pp. 48-66.
[3] J. Bischoff and A.T. Motta, "EFTEM and EELS analysis of the oxide layer formed on HCM12A exposed to SCW", *Journal of Nuclear Materials*, Vol. 430, 2012, pp. 171-180.
[4] I. Pioro, M. Naidin, S. mokry, E. Saltanov, W. Peiman, K. King, A. Farah and H. Thind, "General layouts of supercritical-water NPPS", International Conference on Nuclear Engineering, Proceedings, ICONE 6, 2010, pp. 269-277.
[5] X. Gao, X. Wu, Zh. Zhang, H. Guan and E. Han, " Characterization of oxide films grown on 316L stainless steel exposed to H_2O_2- containing supercritical water", *Journal of Supercritical Fluids*, Vol. 42, 2007, pp. 157-163.
[6] G.S. Was, S. Teysseyre and Z. Jiao, "Corrosion of austenitic alloys in supercritical water", *Corrosion Science*, Vol. 62, No. 11, 2006, pp. 989-1005.
[7] Y. Jiao, S. Mahboubi, J. Kish, W. Cook, W. Zheng and D. Guzonas, "Influence of thermal aging on the corrosion resistance of austenitic Fe-Cr-Ni alloys in SCW", The 6th International Symposium on Supercritical Water-Cooled Reactors, ISSCWR-6, 2013.
[8] S. Ghosh, M. Kiran Kumar and V. Kain, "High temperature oxidation behavior of AISI 304L stainless steel- Effect of surface working operations", *Journal of Applied Science Surface*, Vol. 264, 2013, pp. 312-319.
[9] Y. Nemoto, Y. Miwa, M. Kikuchi, Y. Kaji, T. Tsukada and H. Tsuji, "Development of analytical method and study about microstructure of oxide films on stainless steel", *Journal of Nuclear Science and Technology*, Vol. 39, 2002, pp. 996-1001.
[10] T. Terachi, K. Fujii and K. Arioka, "Microstructural characterization of SCC crack tip and oxide film for SUS 316 stainless steel in simulated PWR primary water at 320 °C", *Journal of Nuclear Science and Technology*, Vol. 42, 2005, pp. 225-232.
[11] W. Kuang, X. Wu and E. Han, "The oxidation behaviour of 304 stainless steel in oxygenated high temperature water", *Corrosion Science*, Vol. 52, 2010, pp. 4081-4087.
[12] A.C.S. Sabioni, A.M. Huntz, F. Silva and F. Jomard, " Diffusion of iron in Cr_2O_3: polycrystals and thin films, *Materials Science and Engineering*, Vol. A 392, 2005, pp. 254-261.
[13] D.S. Williams, R. Möller and H.J. Grabke, "The high -temperature corrosion of Alloy 800 in carburizing, oxidizing and sulfidizing environments", *Oxidation of Metals*, Vol. 16, Nos. 3/4, 1981, pp. 253-266.
[14] D. Young, "High temperature oxidation and corrosion of metals", Elsevier Corrosion Series, First edition, Vol. 1, 2008.
[15] L. Tan, K. Sridharan and T.R. Allen, "The effect of grain boundary engineering on oxidation behaviour of INCOLOY alloy 800H in supercritical water", *Journal of Nuclear Materials*, Vol. 384, 2006, pp. 263-271.

[16] L. Tan, X. Ren, K. Sridharan and T.R. Allen, "Effect of shot-peening on the oxidation of alloy 800H exposed to supercritical water and cyclic oxidation", *Corrosion Science*, Vol. 50, 2008, pp. 2040-2046.
[17] A. T. Motta, A. Yilmazbayhan, M. J. Gomes da Silva, R. J. Comstock, G. S. Was, J. T. Busby, E. Gartner, Q. Peng, Y. H. Jeong, and J. Y. Park, "Zirconium Alloys for Supercritical Water Reactor Applications: Challenges and Possibilities", *Journal of Nuclear Materials*, Vol. 371, 2007, pp. 61-75.
[18] C. Colliex, T. Manoubi and C. Ortiz, "Electron-energy-loss-spectroscopy near-edge fine structures in the iron-oxygen system", *Physics Revolution B (Condense. Matter),* Vol. 44, 1991, pp. 11402-11411.
[19] P. Kofstad, "Non-stoichiometry, diffusion and electrical conductivity inn binary metal oxide", Science and Technology of Materials Series, 1972.
[20] S.C. Tsai, A.M. Huntz and C. Dolin, " Growth mechanism of Cr_2O_3 scales: oxygen and chromium diffusion, oxidation kinetics and effect of yttrium", *Materials Science and Engineering*, Vol. A212, 1996, pp. 6-13.
[21] A. C. S. Sabioni, A. M. Huntz, L. C. Borges and F. Jomard, " First study of manganese diffusion in Cr_2O_3, polycrystals and thin films, by SIMS", *Philosophical Magazine*, Vol. 87, Issue 12, 2007, pp. 1921-1937.
[22] R.E. Lobnig, H.P. Schmidt, K. Hennesen and H.J. Grabke, "Diffusion of cations in chromia layers grown on iron-base alloys", *Oxidation of Metals*, Vol. 37, Issue 1-2, 1992, pp. 81-93.
[23] L. Tan, T.R. Allen and Y. Yang, "Corrosion behavior of alloy 800H (Fe–21Cr–32Ni) in supercritical water", *Corrosion Science*, Vol. 53, 2011, pp. 703-711.